Hindered rotations probed by rare earths in crystals: Er^{3+} and Tm^{3+} in BaY_2F_8

A. Baraldi, E. Buffagni, R. Capelletti,* and M. Mazzera
Physics Department and Consorzio Nazionale Interuniversitario per le Scienze Fisiche della Materia (CNISM), University of Parma, Viale G. P. Usberti 7/A, Campus Universitario, 43124 Parma, Italy

N. Magnani
European Commission, Joint Research Centre, Institute for Transuranium Elements, Postfach 2340, D-76125 Karlsruhe, Germany

G. Carini, Jr. and G. D'Angelo
Physics Department and Consorzio Nazionale Interuniversitario per le Scienze Fisiche della Materia (CNISM), University of Messina, Contrada Papardo, Salita Sperone 31, 98166 S. Agata, Messina, Italy

(Received 7 July 2009; published 14 October 2009)

The sharpness of absorption lines induced by crystal-field (CF) transitions of rare earths (RE) can be exploited to disclose the rotational structure usually hidden under the more common broad electronic absorptions. In the present work the effectiveness of such an approach is proved by the analysis of the fine structure (FS) accompanying the Er^{3+} and Tm^{3+} CF lines in BaY_2F_8 single crystals. Sequences of weak, very narrow (0.03–0.1 cm^{-1}), closely spaced (~0.2–0.8 cm^{-1}) lines were monitored in high-resolution (as fine as 0.01 cm^{-1}), low-temperature (9 K) absorption spectra in the 2000–24 000 cm^{-1} range. The FS covers a few cm^{-1} on both sides of the narrowest among the RE-CF lines and is tightly associated with them, as proved by the amplitude dependence on the RE concentration (in the 0.5–20 at. % range) and by linear dichroism measurements. The FS lines vanishing at temperatures as low as 40–60 K and the close spacing suggest that they may be ascribed to the simultaneous excitation of both RE-CF electronic transition and hindered rotation (or libration) mode of RE^{3+}-F^- group. The attribution is supported both by the specific structure of the host matrix which allows some F^- mobility and by the very small line spacing which is in excellent agreement with the RE^{3+}-F^- rotational constant ($2B$=0.39 cm^{-1}). Complementary specific-heat measurements in the temperature range 1.5–25 K show that Er^{3+}-doped samples display contributions, in addition to the vibrational one of a pure sample, which scale with the Er^{3+} concentration. The extra specific heat is interpreted in terms of Schottky anomalies; that peaking at ~17 K accounts for electronic transitions between the lowest sublevels of the $^4I_{15/2}$ ground manifold, in agreement with the CF spectroscopy results while those occurring below 3.5 K are consistent with level pairs separated by 0.55 and 0.36 cm^{-1}, in agreement with the FS line spacing.

DOI: 10.1103/PhysRevB.80.155121 PACS number(s): 78.30.−j, 42.70.Hj, 71.55.−i

I. INTRODUCTION

As optical active ions or molecular groups are embedded in a solid matrix, the related electronic absorption (or emission) lines broaden due to interaction with lattice vibrations. In addition, the close packing of atoms in solids suppresses, as a rule, some of their degrees of freedom (as, for example, the rotational and vibrational modes). In a way the optical spectra become simpler, by missing the fine structure exhibited by the spectra measured on a low-density gas of the same molecular groups. A photon may simultaneously excite electronic, vibrational, and rotational transitions, giving rise, in the gaseous phase, to complex and line-rich spectra. A very early example is represented by the Schumann-Runge bands of molecular oxygen in the ultraviolet[1] while a recent one deals with high-resolution visible laser spectroscopy of hafnium monofluorides.[2] In a few cases molecular groups retain some mobility, although restricted, even in solids; a demonstration is provided by off-center positions, tunneling, rattling, librations, and hindered rotations, which were put in evidence and investigated by a variety of techniques and have recently opened the way to interesting applications.[3–13]

Under favorable conditions guest ions (or molecules) in a crystal lattice sit in off-center positions; for example, this may happen when the foreign ion size is smaller than that of the host ion it substitutes for. Potential minima, related to off-center positions along equivalent crystal directions, may be deeper than that characterizing the on-center position, thus at low temperatures they may be occupied. Tunneling between minima may occur. Such a description is equivalent, for particular ranges of the parameters, to the hindered rotator or Devonshire model, which starts with a free rotator and adds, for example, a static cubic crystal potential of O_h symmetry;[3,14] states close to or even above the rotational barrier may be excited at relatively low temperatures giving rise to complex and line-rich Raman and infrared (IR) absorption spectra.[15,16] CN^- groups, embedded in potassium halides, behave as nearly harmonic oscillators and simultaneously undergo hindered rotations (or librations) at low temperatures (the related frequency being ~11–12 cm^{-1}); the energy barrier V_0, evaluated in the framework of the Devonshire model, was found to be as small as ~24 cm^{-1}. Tunneling between different minima is monitored by a specific-heat excess peaking at ~0.7 K, which scales with the CN^- concentration.[10]

More recently off-center positions for guest atoms were considered even within the large cages offered by fullerenes; in particular, x-ray diffraction measurements revealed a La "giant motion" in $La@C_{82}$ endohedral metallofullerene, due to an extremely shallow energy barrier.[9] Materials with open

crystal structures, as skutterudites and clathrates, may work as thermoelectrics, when the oversized cages are filled by another type of atoms (e.g., rare earths), with a consequent decrease in thermal conductivity.[4–6,8]

IR spectroscopy allowed monitoring even rotations of polyatomic molecular groups in condensed matter, e.g., NO_2 and NO_3 in alkali-halide single crystals,[10] OCS and SF_6 in liquid He clusters.[13,17] A number of narrow, rotationally resolved side lines, spaced only by ~ 0.02 cm^{-1} and grouped into P and R branches, were detected around the ν_3 vibrational absorption of the SF_6 group.[17]

The spectroscopic evidence for molecular group rotations (both free and hindered) in condensed matter comes mostly from rotovibrational spectra where such modes are simultaneously excited together with the stretching ones.[7,10–13,17–19] Much less is known about rotational or librational lines accompanying electronic transitions, very likely due to the broadness of lines arising from electronic transitions which may cover the finely spaced rotational spectrum. However, a nice example is provided by optical measurements performed on benzoic acid doped with pentacene; the absorption and emission spectra show two line progressions, spaced by 12.2 and 16.7 cm^{-1}, which were attributed to the lowest-frequency libration modes of pentacene in the electronic ground and excited state, respectively.[20] The width of the 16 863 cm^{-1} absorption line, related to the electronic transition of pentacene photosite I, is much smaller (a few cm^{-1}) than the libration-mode frequency, thus allowing the detection of the side lines, see Fig. 3 in Ref. 20.

In the present work the sharpness of absorption lines (as narrow as 0.13 cm^{-1}) originated by electronic transitions of rare earths (RE), as Er^{3+} and Tm^{3+} in BaY_2F_8 single crystals,[21,22] is exploited to probe possible librational or rotational modes. More in detail the fine structure accompanying a few lines, induced by the f-f electronic transitions of Er^{3+} and Tm^{3+}, is analyzed as a function of RE concentration and temperature, by using high-resolution absorption spectroscopy. Such a structure includes a series of weak, extremely narrow (0.03–0.1 cm^{-1}), and closely spaced ($\sim$0.2–0.8 cm^{-1}) lines, covering a few cm^{-1} range on both sides of the narrowest RE zero-phonon (ZP) lines.[21]

BaY_2F_8 single crystals are good rare-earth hosts for laser applications.[23–25] In the monoclinic structure (space group: $C2/m$, lattice parameters: $a=6.9829$ Å, $b=10.519$ Å, $c=4.2644$ Å, $\alpha=\gamma=90°$, and $\beta=99.676°$), Y^{3+} is surrounded by an eight F^- polyhedron.[26] Among the fluorine ions, four are classified as F1, two as F2, and two as F3; they are distinguished by x-ray diffraction analysis performed at room temperature, on the basis of their position, distance from central Y^{3+}, and thermal parameters. Premises to possible librational motion within the eight fluorine cage can be found in some peculiarities of the RE^{3+}-doped BaY_2F_8. The rather large thermal parameter suggests that the F3 anion may be slightly out of the binary axis and may benefit of some mobility. In addition, the F-F distances are larger than the sum of the ionic radii, providing some room for possible F oscillations.[26] Fluorine mobility has been assumed as responsible for BaY_2F_8 ionic conductivity in the temperature range 300–700 K, through a vacancy mechanism;[27] computer modeling has confirmed that Schottky disorder is favored with respect to the Frenkel one.[28] The RE^{3+} substitution for Y^{3+} is supported by the same valency, slightly smaller ionic radius of Er^{3+} and Tm^{3+} with respect to Y^{3+} ($r_Y=1.16$ Å, $r_{Er}=1.14$ Å, and $r_{Tm}=1.13$ Å, respectively),[23] and atomistic modeling.[28] The unnecessary charge compensation enables to reach rather high RE^{3+} doping levels (in the present case up to Er^{3+} 20 at. %), without inducing substantial structural changes.[29] The electronic energy levels of Er^{3+} (a Kramers ion characterized by a $4f^{11}$ configuration) and Tm^{3+} (a non-Kramers ion characterized by a $4f^{12}$ configuration) in BaY_2F_8 have been already thoroughly identified by means of high-resolution spectroscopy and successfully fitted with single-ion model.[21,22] The related crystal-field parameter analysis suggests a distortion of the F^- polyhedron around RE^{3+} and a possible off-center position of RE^{3+} with respect to the original Y^{3+} position.[30]

On the basis of the above considerations, possible librational motions within Er-F_8 and Tm-F_8 polyhedra have been investigated in BaY_2F_8 single crystals, doped with different amounts of Er^{3+} (0.5, 2, 12, and 20 at. %) and Tm^{3+} (0.5, 1, and 5 at. %) by means of high-resolution (as fine as 0.01 cm^{-1}) Fourier transform (FT) spectroscopy in the temperature range 9–300 K. Comparative measurements of low-temperature specific heat have been also performed between 1.5 and 25 K to study the features associated with low-lying excitations between about 0.5 and 50 cm^{-1}, induced by the inclusion of paramagnetic Er^{3+} ions.

II. EXPERIMENTAL DETAILS

The BaY_2F_8 single crystals were grown at the Physics Department of the University of Pisa by a computer-controlled Czochralski technique under a purified argon atmosphere.[31] The samples were prepared from 5N pure BaF_2, Y_2O_3, and RE_2O_3 supplied by AC Materials. The RE^{3+} doping level is given in terms of atomic fraction f_{at}, i.e., the ratio between the numbers of RE^{3+} and Y^{3+} ions. The samples employed in the present work were doped with 0.5, 2, 12, and 20 Er^{3+} at. % and with 0.5, 1, and 5 Tm^{3+} at. %. Nominally pure samples were also analyzed as references. Weak traces of other rare earths (e.g., Nd^{3+}, Ho^{3+}, and Dy^{3+}) could be detected in the samples.[21] For example, the unwanted Er^{3+} concentration in a nominally pure sample was roughly estimated as low as 50 ppm. No trace of OH^- ions was detected, even in samples as thick as 7.5 mm and within the sensitivity limits of the present experimental setup.[21] X-ray diffraction measurements showed that even in highly doped samples (Er^{3+} 20 at. %) no phase separation occurs.[21]

The samples were oriented, cut, and polished for spectroscopic investigation. The sample thickness ranged between 0.9 and 19 mm.

The optical-absorption spectra were monitored by means of a FT spectrophotometer Bomem DA8 operating in the 2000–24 000 cm^{-1} range with a nonapodized resolution as fine as 0.01 cm^{-1}. In the following the absorption lines are labeled by their position (wave number) as measured at 9 K, unless otherwise stated. The sample temperature was controlled in the 9–300 K range by means of a 22 model Cryodine Refrigerator from CTI Cryogenics equipped with KRS5 and fused silica windows.

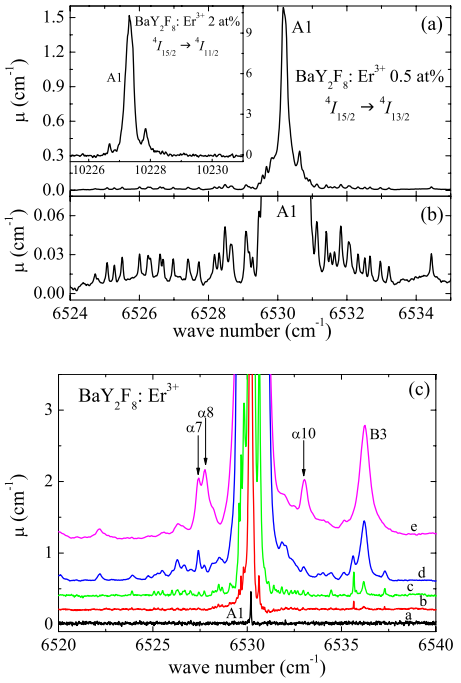

FIG. 1. (Color online) Panel (a): optical-absorption spectrum (resolution=0.04 cm^{-1}) measured at 9 K on a BaY_2F_8:Er^{3+} 0.5 at. % sample in the region of A1 CF line belonging to the $^4I_{15/2} \rightarrow {}^4I_{13/2}$ transition. The inset shows the A1 CF line within the $^4I_{15/2} \rightarrow {}^4I_{11/2}$ transition (resolution=0.04 cm^{-1}). Panel (b): magnification of the weak lines displayed in panel (a), as measured on a thicker sample. Panel (c): optical-absorption spectra, measured at 9 K on BaY_2F_8 samples doped with different Er^{3+} concentrations, in the region of the $^4I_{15/2} \rightarrow {}^4I_{13/2}$ transition. Curve a: nominally pure sample (resolution=0.02 cm^{-1}); curve b: 0.5 at. % (resolution =0.02 cm^{-1}); curve c: 2 at. % (resolution=0.04 cm^{-1}); curve d: 12 at. % (resolution=0.04 cm^{-1}); curve e: 20 at. % (resolution =0.1 cm^{-1}). The solid arrows indicate the α lines due to Er^{3+} clusters. The curves are vertically shifted for clarity.

Measurements with linearly polarized light in the IR region (4000–10 000 cm^{-1}) were performed by using a gold grid polarizer deposited onto a KRS5 substrate; a homemade polarizer holder allowed changing the direction of the light electric field without breaking the vacuum in the spectrophotometer sample compartment.

The specific heat was measured in the 1.5–25 K range using an automated relaxation calorimeter, operating according to the thermal relaxation method. Temperatures were measured by calibrated commercial germanium thermometers. The random error was less than 3–4 %.

III. RESULTS

A. High-resolution optical spectra

1. General features

Figure 1(a) displays the fine structure (FS), which accompanies the line peaking at 6530.2 cm^{-1} (A1 line),[32] originated by the Er^{3+} crystal-field (CF) transition from the lowest sublevel of the $^4I_{15/2}$ ground manifold to the lowest sublevel of the $^4I_{13/2}$ excited manifold, in a BaY_2F_8:Er^{3+} 0.5 at. % single crystal. The absorption spectrum, measured at 9 K with an apodized resolution as fine as 0.04 cm^{-1}, shows on both sides of the A1 line other very weak lines (FS lines); the ratio between the amplitude of the strongest among them, peaking at 6530.63 cm^{-1}, to that of the A1 CF line at 6530.2 cm^{-1} is only 7%. A magnification of the weakest lines is depicted in Fig. 1(b) where the excellent signal-to-noise ratio displayed by the spectra allows distinguishing clearly even the finest details of the structure. In Fig. 1(c) the spectra in the range 6520–6540 cm^{-1} are compared for different Er^{3+} concentrations, i.e., 0.5, 2, 12, and 20 at. %. Also the spectrum of a nominal pure sample is reported; it shows the very weak and narrow (less than 0.045 cm^{-1}) A1 CF line due to traces of Er^{3+}, see Sec. II. FS lines separated only by 0.34–0.4 cm^{-1} from the A1 CF line can be easily distinguished, taking advantage of the high-resolution and low-temperature operation [Fig. 1(b)]. The FS lines cover roughly 5–6 cm^{-1} around the A1 CF line. In Fig. 1(c) curves b (0.5 at. %) and c (2 at. %) show clearly how the FS lines lying on both sides of the A1 CF line increase by increasing the Er^{3+} concentration. In samples with higher Er^{3+} content (i.e., 12 and 20 at. %, curves d and e, respectively) the lines belonging to the fine structure are much stronger, as expected if they are related to the presence of Er^{3+}. However, they are affected both by a relevant inhomogeneous broadening and by the overlapping of bands due to Er clusters (α bands),[21] thus they are less resolved and distinguishable. Examples of α bands, in the spectral range covered by Figs. 1(a)–1(c), are those peaking at 6527.4, 6527.75, and 6533 cm^{-1}, see curves d and e in Fig. 1(c). The band at 6536.2 cm^{-1} is a B3 CF line.[32] The fine structure "decorates" also other Er^{3+} CF lines, either within the $^4I_{15/2} \rightarrow {}^4I_{13/2}$ transition, as, for example, the A2, B1, B2, and C1 lines at 6505.1, 6582.4, 6557, and 6606.2 cm^{-1}, respectively, or within the $^4I_{15/2} \rightarrow {}^4I_{11/2}$ transition, as the A1 line at 10 227.5 cm^{-1} displayed in the inset of Fig. 1(a).[21] However, by increasing the energy of the excited state reached by the CF transition, the width of the related absorption line increases, thus hiding the nearest among the FS lines.

By increasing the temperature at which the spectra are measured, the amplitude of the FS line gradually decreases, see Fig. 2, where the temperature dependence is portrayed for an Er^{3+} 0.5 at. % doped sample, characterized by the best resolved spectra [compare Fig. 1(b) with curves c, d, and e in Fig. 1(c)]. The most of FS lines are no longer detectable yet at 30 K, except for a weak shoulder (overlapped to the A1 CF line at 6530.2 cm^{-1}) reminiscent of the most intense among them (at 6530.63 cm^{-1}). The same trend is monitored in an Er^{3+} 2 at. % doped sample (see Sec. IV and Fig. 6). Different behavior is exhibited by the B3 CF line at 6536.2 cm^{-1}, whose intensity grows due to the thermally activated population increase in the ground manifold excited sublevels (see Fig. 2).

Similar FS patterns accompany the narrowest CF lines induced by Tm^{3+}; an example is supplied in Fig. 3 by curve a, which portrays the 9 K spectrum of a BaY_2F_8:Tm^{3+} 1 at. % sample in the region of the $^3H_6 \rightarrow {}^3F_4$ transition. The two main lines peaking at 5681.85 and 5683.46 cm^{-1} are the A2 and A1 CF lines, respectively; they originate from two transitions reaching the same final state within the excited

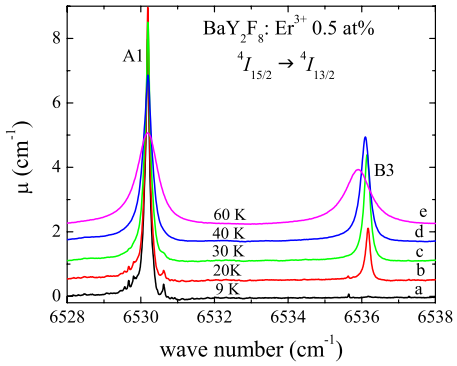

FIG. 2. (Color online) Optical-absorption spectra measured at different temperatures on a BaY_2F_8:Er^{3+} 0.5 at. % sample in the region of the $^4I_{15/2} \rightarrow {}^4I_{13/2}$ transition. Curve a: 9 K (resolution $=0.02$ cm^{-1}); curve b: 20 K (resolution$=0.02$ cm^{-1}); curve c: 30 K (resolution$=0.02$ cm^{-1}); curve d: 40 K (resolution$=0.04$ cm^{-1}); curve e: 60 K (resolution$=0.04$ cm^{-1}). The curves are vertically shifted for clarity.

$^3F_4$ manifold and starting from the first two sublevels (separated by only 1.61 cm^{-1}) of the ground $^3H_6$ manifold.[22] Weak side lines are observed, for example, at 5680.72, 5682.71, and 5684.31 cm^{-1}. The fine structure accompanies also the A1, A2, B1, and B2 CF lines within the $^3H_6 \rightarrow {}^3H_5$ transition (at 8296.8, 8295.1, 8297.5, and 8295.8 cm^{-1}, respectively) and the B1 CF line at 12 662.7 cm^{-1} within the $^3H_6 \rightarrow {}^3H_4$ transition. The FS lines are no longer distinguishable at 60 K, i.e., at a temperature slightly higher than that at which the Er^{3+}-induced FS disappears. As for Er^{3+}-doped samples, the wave number at which the main FS lines fall do not change by changing the Tm^{3+} doping level but they sharpen and weaken by decreasing the RE concentration.

2. Linear dichroism measurements

Spectra measured with linear polarized light emphasize still more the fine structure; a nice example is provided by curves b and c in Fig. 3, related to a BaY_2F_8:Tm^{3+} 1 at. % sample in the region of the $^3H_6 \rightarrow {}^3F_4$ transition and to a light beam traveling along *c* crystallographic direction. This direction was chosen to allow the detection of both the A2 and A1 lines at 5681.85 and 5683.46 cm^{-1}, respectively. Spectra measured with the beam traveling along the *b* axis, i.e., along the principal axis of the index ellipsoid, show only the A1 line, independently of the light polarization. If the electric field of the light, E_l, is perpendicular to the *b* crystallographic direction, the spectrum exhibits a strong A1 line and a weak A2 line, see curve b. On the contrary, if E_l is parallel to the *b* crystallographic direction, the A2 line is very strong while the A1 is weak, see curve c. The polarized spectra reveal more FS lines than the unpolarized spectrum does (see Sec. III A 1), e.g., lines at 5679, 5679.45, 5680.26, 5680.72, 5682.71, 5686.28, and 5686.8 cm^{-1} (see curve c), 5682.4, 5684.31, 5687.27, and 5688.24 cm^{-1} (see curve b). Detailed analysis shows that the lines of the former group exhibit the same angular dependence from E_l as the main A2 CF line does while those of the latter group behave as the A1 CF line [see Sec. IV and Fig. 7(a)]. Even in the case of Er^{3+}-doped BaY_2F_8 samples the polarized light spectra showed that the FS lines exhibit the same angular dependence from E_l of the CF lines they are associated with [see Sec. IV and Fig. 7(b)].

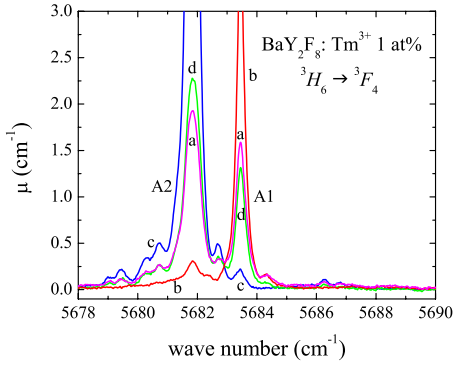

FIG. 3. (Color online) Optical-absorption spectra of a BaY_2F_8:Tm^{3+} 1 at. % sample in the region of the $^3H_6 \rightarrow {}^3F_4$ transition measured at 9 K with linearly polarized light traveling along the *c* axis (resolution$=0.04$ cm^{-1}). Curve a: unpolarized light; curve b: light electric field E_l perpendicular to the *b* axis ($\theta = -90°$); curve c: E_l parallel to the *b* axis ($\theta = 0°$); curve d: $\theta = -45°$.

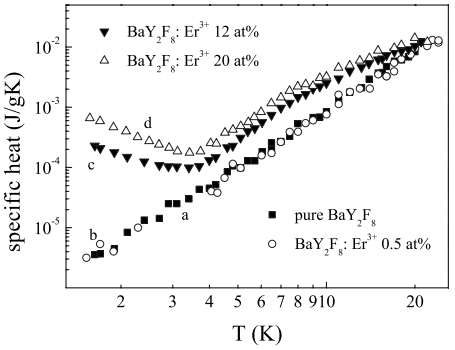

FIG. 4. Specific heat measured as a function of temperature in the range 1.5–22 K on different BaY_2F_8 samples. Curve a (squares): nominally pure sample; curve b (circles): Er^{3+} 0.5 at. %; curve c (full triangles): Er^{3+} 12 at. %; curve d (empty triangles): Er^{3+} 20 at. %.

B. Specific-heat measurements

Above 20 K the specific heat (C_p) is nearly the same for BaY_2F_8 samples both pure and doped with different Er^{3+} concentrations (Fig. 4), suggesting that only lattice vibrational contributions are responsible for C_p. Below 20 K, the specific heat of the samples containing relevant amounts (12 and 20 at. %) of Er^{3+} exceeds that of the undoped one, becoming about two orders of magnitude larger at the lowest temperatures. As a rule, C_p of insulating crystals doped with paramagnetic ions may include, below 20 K, a contribution C_{CF}, coming from the crystal field, in addition to the vibrational one C_{Vib}, i.e., $C_p = C_{Vib} + C_{CF}$. In the present case crystal field removes the degeneracy of the Er^{3+} lowest-lying manifold $^4I_{15/2}$ and splits it into eight Kramers doublets. In insulating crystals phonons usually dominate the thermal properties: both pure BaY_2F_8 sample and that doped with

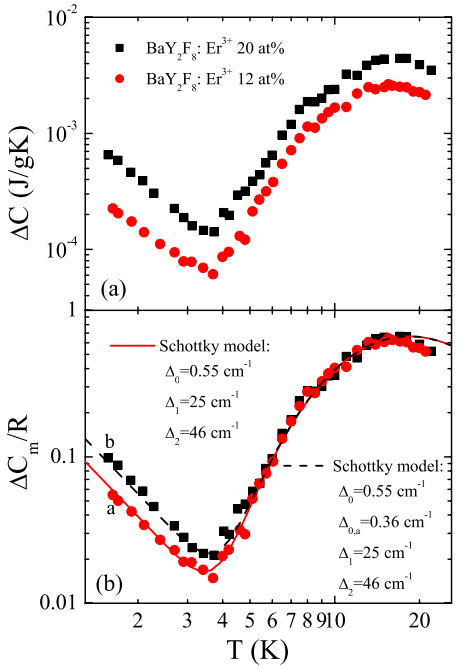

FIG. 5. (Color online) Panel (a): temperature dependence of the excess contribution to the specific heat, $\Delta C \equiv (C_{\mathrm{Er}} - C_{\mathrm{Y}})$, of two BaY_2F_8 samples doped with different Er^{3+} concentrations: 12 at. % (circles) and 20 at. % (squares). Panel (b): temperature dependence of the excess contributions to the specific heat per Er^{3+} mole (ΔC_{m}) divided by R with respect to a nominally pure sample of two BaY_2F_8 samples doped with different Er^{3+} concentrations: 12 at. % (curve a, circles) and 20 at. % (curve b, squares). The solid and dashed lines are the results of different approaches according to the Schottky model by using three and four energy splittings, respectively.

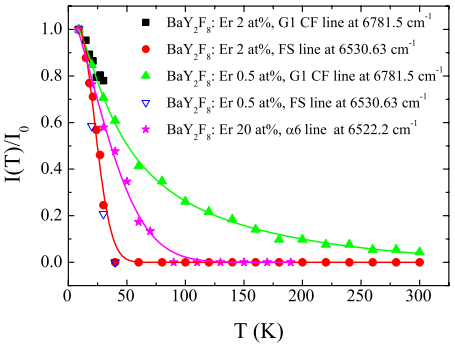

FIG. 6. (Color online) Temperature dependence of the amplitude for a few lines detected in BaY_2F_8 samples doped with different Er^{3+} concentrations. Squares: G1 CF line (2 at. %); circles: FS line at 6530.63 cm^{-1} (2 at. %); full triangles: G1 CF line (0.5 at. %); empty triangles: FS line at 6530.63 cm^{-1} (0.5 at. %); stars: $\alpha 6$ line at 6522.2 cm^{-1} (20 at. %). The solid lines are guides for the eyes.

only Er^{3+} 0.5 at. % show a C_{p} which, below 12 K, follows strictly the Debye T^3 law (see Fig. 4). From the slope of the related straight line in the log-log plot a Debye temperature $\theta_D = 388$ K can be extracted. To estimate the C_{p} excess displayed by Er^{3+} (12 and 20 at. %) doped samples and its temperature dependence, the specific heat of the undoped sample is assumed to supply the vibrational contribution. This is acceptable because Er^{3+}-doped and undoped BaY_2F_8 crystals have the same structure, as supported by x-ray diffraction measurements.[21] Furthermore rather small differences in the crystal compositions (Er^{3+} substitutes for Y^{3+}) are not expected to change significantly the vibrational contributions.[29] The subtraction of the undoped sample specific heat ($C_{\mathrm{Y}} \equiv C_{\mathrm{Vib}}$) from that of the samples containing paramagnetic ions (C_{Er}), provides an estimate of the anomalous contribution, $\Delta C \equiv (C_{\mathrm{Er}} - C_{\mathrm{Y}})$. The temperature dependence of ΔC for the two Er^{3+}-doped samples is reported in Fig. 5(a). Both contributions exhibit a bump at about 17 K, whose magnitude increases by increasing the Er^{3+} concentration, and a further upturn at temperatures lower than about 3.5 K, which follows a T^{-2} dependence [Figs. 4 and 5(b)]. It is worth noting that the higher the temperature the larger is the error which affects the ΔC evaluation because C_{Vib} becomes dominant over C_{CF} in determining C_{p}. Despite this difficulty, the characteristics of the maximum are well defined and significantly above the error; data taken in different experimental runs always reproduced the same trend.

IV. DISCUSSION

The FS lines detected in BaY_2F_8 doped either with Er^{3+} or Tm^{3+} display common features. (1) They are monitored on both sides of the narrowest CF lines because their separation from the CF line may be as small as ~ 0.4 cm^{-1}, thus larger than the CF line width. (2) They "decorate" lines originated by CF transitions both from the lowest and from the first-excited sublevel of the ground manifold to different sublevels of the excited manifolds (X1 and X2 lines, respectively). (3) They are related to the RE^{3+}, in fact they do not appear in a nominally pure sample and their amplitude (and, unfortunately, their width too) increases by increasing the RE^{3+} concentration [see, for example, Fig. 1(c)]. (4) They are no longer detectable yet at rather low temperatures (40 and 60 K for Er^{3+} and Tm^{3+}-doped samples, respectively), see Fig. 2, i.e., at temperatures much lower than those at which the CF lines broaden and weaken, see Fig. 6. The latter compares, as a function of temperature, the amplitudes of (a) the line at 6530.63 cm^{-1}, i.e., the strongest among the FS lines accompanying the A1 CF line at 6530.2 cm^{-1}, (b) a G1 CF line at 6781.5 cm^{-1}, for two different Er^{3+} concentrations, i.e., 0.5 and 2 at. %, respectively, and (c) the α line peaking at 6522.2 cm^{-1}, i.e., a line related to a RE cluster in a heavily (20 at. %) doped sample. The G1 line is chosen as representative of the CF lines, instead of the A1 because its amplitude is comparable with that of the FS line at 6530.63 cm^{-1} while that of the A1 is very high, thus cannot be evaluated correctly over the whole temperature range, being affected by the detector nonlinearity.[21] The figure shows very clearly that the FS-line amplitude exhibits much faster temperature decay than the G1 CF line (for both Er^{3+} doping levels) and the α line peaking at 6522.2 cm^{-1}. (5) The FS lines and the CF lines, they are associated with, show the same behavior as a function of the polarization angle θ (with respect to the b axis), see Fig. 3 for a sample doped with Tm^{3+} 1 at. % and for $\theta = -90$, -45, and $0°$, respectively. A more comprehensive

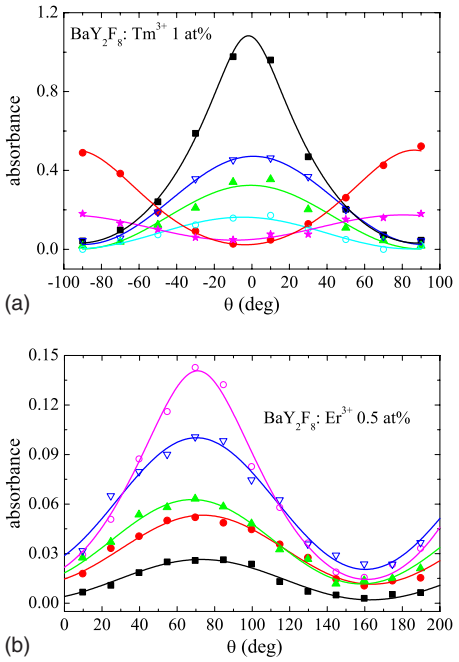

FIG. 7. (Color online) Angular dependence on the light electric field E_l for a few lines detected in the spectra measured at 9 K. Panel (a): BaY_2F_8:Tm^{3+} 1 at. % sample in the region of the $^3H_6 \rightarrow {}^3F_4$ transition. The beam travels along the c axis and θ is the angle between E_l and the b axis. Squares: A2 CF line; full circles: A1 CF line; full triangles: FS line at 5679.45 cm^{-1} (multiplied by a factor 10); empty triangles: FS line at 5680.72 cm^{-1} (multiplied by a factor 10); empty circles: FS line at 5686.28 cm^{-1} (multiplied by a factor 10); stars: FS line at 5688.24 cm^{-1} (multiplied by a factor 40). The solid lines are guides for the eyes. Panel (b): BaY_2F_8:Er^{3+} 0.5 at. % sample in the region of the $^4I_{15/2} \rightarrow {}^4I_{13/2}$ transition. The beam travels along the b axis and θ is the angle between E_l and the c axis. Squares: FS line at 6529.57 cm^{-1}; full circles: FS line at 6529.67 cm^{-1}; full triangles: FS line at 6529.82 cm^{-1}; empty triangles: FS line at 6530.63 cm^{-1}; empty circles: A1 line (multiplied by a factor 2). The solid lines are guides for the eyes.

picture is given in Fig. 7 both for Er^{3+} and Tm^{3+} doping. In Tm^{3+}-doped sample [Fig. 7(a)] the A1 CF line at 5683.46 cm^{-1} displays a maximum for $\theta = \pm 90°$ and a minimum at 0°; the same trend is exhibited by the very weak FS line at 5688.24 cm^{-1}. The FS lines peaking at 5679.45, 5680.72, and 5686.28 cm^{-1}, appearing on both sides of the A2 line at 5681.85 cm^{-1}, and the A2 line itself show an opposite trend. Similar behavior is observed in Er^{3+}-doped samples [Fig. 7(b)]; all the FS lines show the same angular dependence as the CF lines they decorate. More in detail, the FS lines at 6529.57, 6529.67, 6529.82, and 6530.63 cm^{-1} accompanying the A1 CF line at 6530.2 cm^{-1} exhibit the same trend as the A1 line does, with a maximum at ~72° (with respect to the c axis) and a minimum at ~162°. The A1 CF line behavior is monitored by plotting the amplitude taken not at the peak (either out of scale or affected by the detector nonlinearity because too high) as for the weak FS lines but on the line tail at 0.1 cm^{-1} from the peak position, where no FS line contributes to the absorption.

The polarization angle at which the maximum occurs allows identifying the position of the principal axis of the index ellipsoid but does not provide any information about the orientation of the dipole moment associated with a given transition.[33] This can be estimated from the ratio between the maximum and the minimum of the line amplitude vs polarization angle plots.[33] On this basis the data displayed in Fig. 7(b) were analyzed; the angle between principal axis and the dipole moment associated with each of the FS lines at 6529.57, 6529.67, 6529.82, and 6530.63 cm^{-1} is, within the experimental error, the same as that associated to the A1 CF line they accompany. Such a finding supports once more the close relation between the FS lines and the CF they decorate. Which is the origin of the weak FS lines? For Er^{3+}-doped samples, the FS-line pattern and spacing can be accounted for neither by hyperfine interaction between the nuclear spin ($I=7/2$) of ^{167}Er (natural abundance 22.94%) and the electronic total angular moment nor by isotopic effects due to the presence, in addition to ^{167}Er, of ^{166}Er, ^{168}Er, and ^{170}Er of comparable natural abundance (33.41%, 27.07%, and 14.88%, respectively). The number of lines expected is $2I+1$, i.e., 8 for ^{167}Er on the basis of hyperfine interaction and one for each Er^{3+} isotope, as in the case of Er^{3+}-doped $LiYF_4$ tetragonal single crystals,[34] thus the total number is much lower than that of the FS lines actually monitored. Furthermore hyperfine interaction should be excluded because once the values of the coupling constants for a given RE and the CF eigenfunctions of that RE in the host crystals[21] are known, its associated features and energy splittings should follow determinate quantitative and qualitative patterns[35,36] which are not compatible with the present observations. Similar considerations can be applied to rule out the hyperfine interaction as responsible for the FS in the case of ^{169}Tm (100% natural abundance, $I=1/2$) doped samples.[22,35]

The FS lines cannot be induced by vibronic transitions, i.e., transitions in which a photon and a phonon are simultaneously absorbed[37,38] because the separation of the strongest among the FS lines from the ZP lines is extremely small (on the order of a few tenths of cm^{-1}, i.e., $\sim 10^{-4}$ eV); the density of states for lattice modes of such low energies is negligible.

The FS lines might also be considered as satellite lines related to RE^{3+}-RE^{3+} interaction or to the presence of isolated perturbed sites (e.g., vacancies or interstitial ions). As displayed in Fig. 6 the temperature dependence of the amplitude of the FS lines is quite different from that of the α line related to RE clusters,[21] therefore suggesting a different origin for the two sets of lines. On the other hand the random distribution of isolated perturbed sites is expected to induce an inhomogeneous broadening of the CF lines rather than the well-defined FS line pattern; in addition since RE^{3+} substitutes for the homovalent Y^{3+} (see Sec. I), the charge compensation defects are not required. Thus, no defect is expected to neighbor the RE^{3+}, as, for example, in the case of divalent cations doped in alkali halides, where the charge compensating cation vacancy gives rise to divalent impurity-cation vacancy complexes (see, for example, Introduction in Ref. 21). Furthermore, the statistical weight of satellite lines related to defects should change from sample to sample. On the contrary, the FS pattern does not change for different samples either taken from different parts of the same ingot [0.5 at. %, compare in Fig. 1 the curve displayed in panel

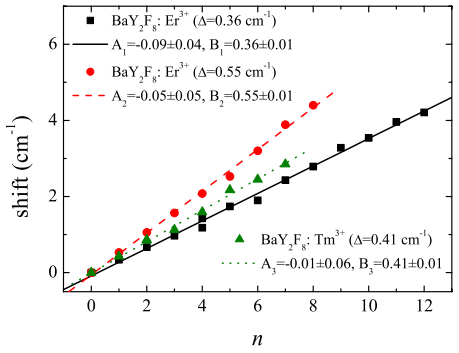

FIG. 8. (Color online) FS-line sequences observed in BaY_2F_8 samples doped with Er^{3+} (squares and circles) and Tm^{3+} (triangles). The separation of the FS lines from the related CF is plotted vs a quantum number n. The straight lines are the linear fits ($y=A_i+B_ix$) of the experimental data.

(b), for a thick sample, with curve b in panel (c), for a thin sample] or of different doping level [2 at. %, see curve c in Fig. 1(c)].

More likely the FS lines might be attributed to a simultaneous excitation both of an electronic and a local mode. Due to the small energy quanta involved ($\sim 10^{-4}$ eV), possible candidates for local modes are (hindered) rotations or librations of RE-F groups. Thus the data analysis was performed as follows. The separations of the FS lines from the related CF ones were collected for all the CF lines and for samples with different RE^{3+} concentrations. Some of the lines are located symmetrically, i.e., at the same distance on both sides of a given CF line. The presence of FS lines even at energies lower than the CF ones in the 9 K spectra is consistent with the fact that possible rotational-like excited states may be already populated at low T, due to their small separation from the ground state. The separation values of the FS lines, which are symmetric with respect to the CF line they decorate and common to more than one CF line, were selected (due to their large statistical weight) and were plotted as a function of an integer number (quantum number) n. The result is displayed in Fig. 8. For Er^{3+}-doped samples two sequences of nearly equispaced FS lines are identified by the two straight lines which converge in the origin; their slopes are (0.36 ± 0.01) and (0.55 ± 0.01) cm^{-1}, respectively. An equispaced FS-line sequence, as for OCS molecules in He droplets, suggests a free-rotatorlike behavior;[17] if this is the case, the straight-line slope provides the separation $2B$, where B is the rotational constant, i.e., $B \equiv \hbar^2/(2M_I)$, with $\hbar$ the reduced Planck's constant and M_I the moment of inertia. As already mentioned in Sec. I, among the eight F^- ions surrounding every Y^{3+}, and consequently every Er^{3+} which replaces Y^{3+}, the F3 anion may benefit of some mobility. From the separation Y^{3+}-F3 (or Er^{3+}-F3) $d=2.242 \times 10^{-8}$ cm and the Er^{3+} and F^- masses, $2B$ for the Er^{3+}-F3 complex can be easily evaluated as 0.39 cm^{-1}.[26] Not only the order of magnitude but also the numerical value is in excellent agreement with those supplied by the straight-line slopes in Fig. 8, notwithstanding the oversimplified model. Calculation of $2B$ for Er^{3+}-F1 and Er^{3+}-F2 complexes provides comparable values. This strengthens the attribution of the FS to a simultaneous excitation of an electronic and a local rotational-like mode of an Er^{3+}-F^- complex. Similar results were obtained from the analysis of the FS in Tm^{3+}-doped samples. The FS-line separations from the A1, A2, B1, and B2 CF lines within the $^3H_6 \rightarrow {}^3H_5$ transition (at 8296.8, 8295.1, 8297.5, and 8295.8 cm^{-1}, respectively) in a Tm^{3+} 5 at. % doped sample plotted as a function of a quantum number n provided a straight line whose slope is (0.355 ± 0.003) cm^{-1}. The same procedure applied to the closest among the FS lines associated with the A1 and A2 CF lines at 5683.46 and 5681.85 cm^{-1} ($^3H_6 \rightarrow {}^3F_4$ transition in BaY_2F_8:Tm^{3+} 1 at. %, see Fig. 3) originated the straight line displayed in Fig. 8; the slope is (0.41 ± 0.01) cm^{-1}.

Therefore, the rotational constants B, as deduced from the FS-line sequences, are ~0.18 and 0.28 for Er^{3+}-F^- and 0.18 and 0.21 cm^{-1} for Tm^{3+}-F^- complexes, respectively, in BaY_2F_8. Such values are close to those falling in the 0.26 and 0.28 cm^{-1} range, estimated from the rotational analysis of high-resolution laser excitation spectra originated by different electronic transitions of gaseous HfF.[2] Although the similarity of the rotational constants might be expected on the basis of comparable moment of inertia of Er^{3+}-F^-, Tm^{3+}-F^-, and Hf-F molecular groups, the result confirms the rotational origin of the FS lines in Er^{3+}- and Tm^{3+}-doped BaY_2F_8. Between the two B values, i.e., ~0.18 and 0.28 cm^{-1}, provided by the FS-line progressions in Fig. 8 for Er^{3+}-doped BaY_2F_8, the latter suggests a lower moment of inertia with respect to that calculated above (~0.20 cm^{-1}) on the basis of the available data for the Er-F separations.[26] Such data originate from x-ray diffraction measurements performed at room temperature (RT) while the FS lines are monitored at 9 K; a not necessarily isotropic shrinking of the BaY_2F_8 unit cell occurring by the temperature lowering might be responsible for some Er-F separation shortening and, consequently, for the moment of inertia decrease. As a matter of fact, the thermal-expansion coefficient is known to be anisotropic already around RT (i.e., 17, 18.7, and 19.4 $\times 10^{-6}$ K^{-1} along the a, b, and c directions, respectively).[39] In addition, a distortion of the F^- polyhedron around Er^{3+} and a possible off-center position of Er^{3+} with respect to the original Y^{3+} position are suggested by crystal-field parameter analysis.[30]

Further support comes from the analysis of the specific-heat excess detected in Er^{3+}-doped samples, see Sec. III B and Fig. 5. The specific-heat excess divided by the nominal number of Er^{3+} moles and by R (the universal gas constant), i.e., $(C_{Er,m}-C_{Y,m})/R \equiv \Delta C_m/R$, is displayed in Fig. 5(b) for the two samples, doped with 12 and 20 at. % nominal Er^{3+} concentration. Within the experimental error, the data overlap, showing that ΔC scales with Er^{3+} concentration; the agreement is particularly good at $T>5$ K. Both the low- (below 3.5 K) and high-temperature (at about 17 K) contributions to ΔC_m exhibit the characteristics of a Schottky anomaly, which is well known to grow exponentially with temperature and, at sufficiently high temperatures, to decrease as T^{-2}. Thus, the influence of the low-temperature anomaly on the maximum amplitude of the high-temperature one is small. The high-temperature anomaly displays its maximum at about 17 K, which corresponds to a splitting of about 40.9 K or 28.4 cm^{-1}, a value little higher than that (25 cm^{-1}) determined from optical spectroscopy measure-

ments and associated with the electronic transitions between the two lowest-lying Kramers doublets within the ground $^4I_{15/2}$ manifold.[21] The maximum amplitude of $\Delta C_m/R$ at about 17 K ranges between 0.61 and 0.66, a value higher than that (0.44) expected for the simplest case of two levels with equal degeneracy and separated by a quantity Δ_i. Consequently the electronic transitions toward the second-excited doublet above the ground state are also considered. On the basis of the energy-level scheme for CF transitions,[21] the next step is to calculate $\Delta C_m/R$ from the appropriate partition function for two Kramers doublets separated by Δ_1 and Δ_2 from the ground one. The T^{-2} behavior of ΔC_m observed below 3 K is accounted for by considering the high-temperature tail of a single Schottky anomaly with a Δ_0 splitting. The following expression for the specific heat is deduced:

$$\frac{\Delta C_m}{R} = \left(\frac{\Delta_0}{2T}\right)^2 + \left\{ \frac{\left(\frac{\Delta_1}{T}\right)^2 \exp\left(-\frac{\Delta_1}{T}\right) + \left(\frac{\Delta_2}{T}\right)^2 \exp\left(-\frac{\Delta_2}{T}\right) + \left(\frac{\Delta_2 - \Delta_1}{T}\right)^2 \exp\left(-\frac{\Delta_1 + \Delta_2}{T}\right)}{\left[1 + \exp\left(-\frac{\Delta_1}{T}\right) + \exp\left(-\frac{\Delta_2}{T}\right)\right]^2} \right\}. \quad (1)$$

$\Delta C_m/R$ has been evaluated according to Eq. (1) by using the Δ_i splittings, deduced from spectroscopy measurements, i.e., $\Delta_0=0.79$ K (0.55 cm^{-1}), $\Delta_1=36$ K (25 cm^{-1}), and $\Delta_2=66.2$ K (46 cm^{-1}); the resulting curve is shown as a solid line in Fig. 5(b). By considering that the accuracy of the $\Delta C \equiv (C_{Er}-C_Y)$ values decreases with rising temperature above about 17 K, the numerical evaluation according to Eq. (1) may be assumed as a satisfactory quantification of $\Delta C_m/R$, over the whole investigated temperature range for the sample doped with Er^{3+} 12 at. % [curve a in Fig. 5(b)] and for $T>3.5$ K for that doped with Er^{3+} 20 at. % [curve b in Fig. 5(b)]. The experimental data related to the sample doped with Er^{3+} 20 at. % can be satisfactorily reproduced even in the low-temperature range (see dashed line) by using Eq. (1) with the same set of Δ_i values used above and by adding a low-temperature Schottky anomaly characterized by a $\Delta_{0,a}=0.52$ K (0.36 cm^{-1}), suggested again by IR spectroscopy measurements (Fig. 8). The difference between the curves a and b for $T<3.5$ K can be tentatively explained by the increased statistical weight of Er clusters in Er^{3+} 20 at. % doped sample; they are monitored by the α lines in optical spectra [compare curves d and e in Fig. 1(c)]. The separation between the electronic sublevels of clusters (e.g., Δ_1) is quite close to that of isolated Er^{3+}, see Table VII in Ref. 21, thus the CF contribution to $\Delta C_m/R$ remains practically unchanged. On the contrary, the rotational-like frequencies of Er^{3+}-F^- groups, related to the moment of inertia, may be more significantly affected, for example, by the slight lattice distortions caused by an additional neighboring Er^{3+}.

The striking agreement between the energies (25 and 46 cm^{-1}) associated with the high-temperature Schottky anomaly and those obtained from spectroscopy measurements, shows that anomalous specific heat at $T>3.5$ K is determined by the electronic transitions between the three lowest-lying sublevels. The level separation of a few tenths of cm^{-1} [$\Delta_0=0.55$ cm^{-1} for curve a and $\Delta_0=0.55$ and $\Delta_{0,a}=0.36$ cm^{-1} for curve b in Fig. 5(b)] extracted from the T^{-2} behavior, monitored at $T<3.5$ K and ascribed to high-temperature tail of Schottky anomalies, seems to be a strong evidence for a contribution given by rotational-like levels of the Er-F complex. Unfortunately, the limited temperature range explored (down to 1.5 K) prevents an exhaustive evaluation of the magnitude of the low-temperature Schottky anomalies and an extension to lower temperatures of the present work should be surely useful in the interpretation of this latter point.

Specific-heat measurements on Tm^{3+}-doped samples were deliberately not performed because the separation between the two lowest sublevels of the ground $^3H_6$ manifold is only 1.6 cm^{-1} (Ref. 22); the electronic contribution is expected to overlap that coming from the rotational-like levels ($\Delta=0.36-0.41$ cm^{-1}, see above), thus precluding any clear-cut interpretation.

In spite of the overall self-consistency of the description supplied, some criticisms and refinements may be put forth: (1) the description of Er^{3+}-F^- complex as a free rotator is naïve; more likely the Er^{3+}-F^- (or Tm^{3+}-F^-) complex mobility should be more restricted and characterized by hindered rotations and/or librations and (2) a few of the FS lines actually monitored by the spectra do not fit in the scheme supplied by Fig. 8.

Beyeler[15,16] has calculated the vibration-rotation absorption spectra of "rotator" hindered by fields of cubic symmetry for different values (and geometries) of the energy barrier, separating potential minima, and for different temperatures. The simulation supplies line-rich spectra, which resemble closely those accompanying the RE^{3+} CF lines in the present work. The lines are not equally spaced, unless the barrier vanishes and/or the temperature is high enough to allow "free rotations." At low temperatures the lines are fewer and some are due to librations of the molecular group within the potential wells; in this case the librational absorption lines appear on the high-energy side, well separated from the central line. For $k_BT \ll V_0$, where V_0 is the energy barrier, the molecular group occupies levels below the top of the barrier and the energy levels are those of a harmonic oscillator of frequency ν_{libr} which depends on V_0 and on the rotational constant B as

$$\nu_{libr} = 2(V_0 B)^{1/2}, \quad (2)$$

where ν_{libr}, V_0, and B are expressed in cm^{-1}.[10,40] Thus the physical picture is that of a molecular group executing a rocking motion with its own energy levels and statistical thermodynamic functions.[41]

Tunneling across the energy barrier is also expected. There is no contradiction between the two descriptions: the closely spaced energy levels of hindered rotator (a model suitable for low or medium potential-energy barriers) converge to those expected on the basis of tunneling between different minima (suitable for higher-energy barriers).[16,42] The hindered-rotator model expresses the rotational motion as a linear combination of spherical harmonic wave functions while the tunneling model calculates the same energy levels by allowing localized harmonic-oscillator wave functions to overlap the equivalent wave functions in neighboring potential wells.[42]

In the case of $BaY_2F_8:Tm^{3+}$, in addition to the closely spaced FS lines overlapping the A2 and A1 CF lines at 5681.85 and 5683.46 cm^{-1}, respectively, there are two groups of much weaker FS lines on the higher-energy side, separated from the A1 and A2 lines by about 4.5 and 4.7 cm^{-1}, respectively, see Fig. 3. The main lines of the two groups peaking at 5686.28 and 5688.24 cm^{-1}, respectively, exhibit the same polarization dependence as the A1 and A2 lines do, see Fig. 7(a); they might be regarded as librational lines associated with the A1 and A2 lines. Equation (2) was originally obtained by Pauling[40] for a potential $V=\frac{1}{2}V_0(1-\cos 2\vartheta)$, where ϑ is the angle between the molecular group and a reference axis. Such a potential is not necessarily the same probed by the Tm^{3+}-F^- complex in BaY_2F_8, however V_0 may be roughly estimated by assuming librational frequencies $\nu_{libr}=4.5$ and 4.7 cm^{-1} and $2B=0.41$ cm^{-1} (see above). The resulting values of V_0 are about 25 and 27 cm^{-1}, i.e., the energy barrier "seen" by the librating Tm^{3+}-F^- molecular group, when the Tm^{3+} electronic transition starts from the first-excited sublevel and from the lowest one within the ground $^3H_6$ manifold, respectively, to reach the first sublevel of the excited $^3F_4$ manifold (A2 and A1 lines). The low values of V_0 (on the order of 3×10^{-3} eV) explain why the FS lines are no longer detectable yet at $T>60$ K (see Sec. III A 1), due also to the thermally induced line broadening. At high temperature the Tm^{3+}-F^- molecular group experiences a precession around a fixed axis; a thermally activated process makes it able to pass over the barrier which separates different angular positions, corresponding to the potential minima. However the typically free-rotator line spectrum cannot be detected due to the simultaneous line broadening. At low temperatures the barrier can be crossed only by tunneling and the Tm^{3+}-F^- molecular group performs only small angular oscillations (librations) within the well.

In $BaY_2F_8:Er^{3+}$ spectra it is difficult to identify unequivocally a librational line, from whose position V_0 might be, at least roughly, estimated according to Eq. (2). The Er^{3+} FS lines are no longer distinguishable at temperatures as low as 40 K (see Sec. III A 1 and Fig. 2): this suggests that the energy barrier which separates different orientations of the Er^{3+}-F^- complex is still less than that estimated for the Tm^{3+}-F^- complex. Thus 9 K can be regarded as a temperature high enough to forbid the librational line detection.

V. CONCLUSIONS

By taking advantage of high-resolution measurements performed at low temperatures, the very narrow lines induced by crystal-field transitions of RE^{3+}, as Er^{3+} and Tm^{3+} in BaY_2F_8, are exploited as a probe to put in evidence and study "rotoelectronic" transitions even in solids, where, as a rule, such fine details are masked by the broadness of the lines arising from purely electronic transitions. The sequences of very weak, finely spaced lines "decorating" both sides of the main CF lines are interpreted as due to photons exciting simultaneously a CF transition and a rotational-like mode of RE^{3+}-F^- group. These modes are characterized by very small energies (a few tenths of cm^{-1}), as expected on the basis of the RE^{3+}-F^- moment of inertia and supported, in the case of Er^{3+}-doped BaY_2F_8, also by the low-temperature Schottky anomalies appearing in the specific-heat plots.

The present results may open a way to disclose and analyze even subtle effects, as the low-energy rotational dynamics of atoms/ions neighboring the RE in solid matrices, providing more direct and detailed information with respect to that supplied by rotovibrational spectroscopy, where the rotational contribution must be extracted from a complex, structured, and still broad line shape.[7,11,12,18,19] The superior resolution offered by FTIR spectroscopy applied to RE with respect to the neutron scattering might solve the still open problem of RE^{3+} rattling in skutterudites.[6]

ACKNOWLEDGMENTS

The authors would like to express their gratitude to Mauro Tonelli and co-workers (Physics Department, University of Pisa) for providing BaY_2F_8 single crystals and to Carlo Mora (IMEM-CNR, Parma) for technical help. N.M. acknowledges the European Commission for support given in the frame of the program "Training and Mobility of Researchers."

*rosanna.capelletti@fis.unipr.it

[1] H. P. Knauss and S. S. Ballard, Phys. Rev. **48**, 796 (1935).
[2] A. G. Adam, W. S. Hopkins, and D. W. Tokaryk, J. Mol. Spectrosc. **225**, 1 (2004).
[3] F. Bridges, Crit. Rev. Solid State Mater. Sci. **5**, 1 (1975).
[4] V. Keppens, D. Mandrus, B. C. Sales, B. C. Chakoumakos, P. Dai, R. Coldea, M. B. Maple, D. A. Gajewski, E. J. Freeman, and S. Bennington, Nature (London) **395**, 876 (1998).

[5] R. P. Hermann, R. Jin, W. Schweika, F. Grandjean, D. Mandrus, B. C. Sales, and G. J. Long, Phys. Rev. Lett. **90**, 135505 (2003).
[6] M. M. Koza, M. R. Johnson, R. Viennois, H. Mutka, L. Girard, and D. Ravot, Nature Mater. **7**, 805 (2008).
[7] K. R. Martin, C. Peng, S. Kleekajai, P. Blaney, E. Diamond, W. B. Fowler, M. Stavola, and R. González, Physica B (Amsterdam) **401-402**, 421 (2007).
[8] R. Baumbach, F. Bridges, L. Downward, D. Cao, P. Chesler, and B. Sales, Phys. Rev. B **71**, 024202 (2005).
[9] E. Nishibori, M. Takata, M. Sakata, H. Tanaka, M. Hasegawa, and H. Shinohara, Chem. Phys. Lett. **330**, 497 (2000).
[10] W. D. Seward and V. Narayanamurti, Phys. Rev. **148**, 463 (1966); V. Narayanamurti, W. D. Seward, and R. O. Pohl, *ibid.* **148**, 481 (1966).
[11] M. Krantz and F. Luty, Phys. Rev. B **37**, 7038 (1988).
[12] G. A. Shi, M. Stavola, W. B. Fowler, and E. E. Chen, Phys. Rev. B **72**, 085207 (2005).
[13] S. Grebenev, M. Hartmann, M. Havenith, B. Sartakov, J. P. Toennies, and A. F. Vilesov, J. Chem. Phys. **112**, 4485 (2000), and references therein.
[14] V. Narayanamurti and R. O. Pohl, Rev. Mod. Phys. **42**, 201 (1970).
[15] H. U. Beyeler, Phys. Rev. B **10**, 2614 (1974).
[16] H. U. Beyeler, J. Chem. Phys. **60**, 4123 (1974).
[17] M. Hartmann, R. E. Miller, J. P. Toennies, and A. Vilesov, Phys. Rev. Lett. **75**, 1566 (1995).
[18] S. Ludwig, A. Brederek, C. Enss, C. P. An, and F. Luty, Phys. Rev. Lett. **85**, 5591 (2000).
[19] S. Kapphan and F. Luty, Phys. Rev. B **6**, 1537 (1972).
[20] L. W. Molenkamp and D. A. Wiersma, J. Chem. Phys. **80**, 3054 (1984).
[21] A. Baraldi, R. Capelletti, M. Mazzera, A. Ponzoni, G. Amoretti, N. Magnani, A. Toncelli, and M. Tonelli, Phys. Rev. B **72**, 075132 (2005).
[22] A. Baraldi, R. Capelletti, M. Mazzera, P. Riolo, G. Amoretti, N. Magnani, E. Sani, A. Toncelli, and M. Tonelli, Phys. Status Solidi C **2**, 248 (2005).
[23] A. A. Kaminskii, *Laser Crystals*, 2nd ed. (Springer-Verlag, Berlin, 1990); A. A. Kaminskii, *Crystalline Lasers: Physical Processes and Operating Schemes* (CRC, New York, 1996).
[24] A. A. Kaminskii, Laser Photonics Rev. **1**, 93 (2007).
[25] M. Pollnau, W. Lüthy, H. P. Weber, T. Jensen, G. Huber, A. Cassanho, H. P. Jenssen, and R. A. Macfarlane, Opt. Lett. **21**, 48 (1996).
[26] L. H. Guilbert, J. Y. Gesland, A. Bulou, and R. Retoux, Mater. Res. Bull. **28**, 923 (1993).
[27] V. Trnovcová, P. P. Fedorov, A. A. Bystrova, T. Šrámková, and B. P. Sobolev, Solid State Ionics **106**, 301 (1998).
[28] J. B. Amaral, M. A. Couto Dos Santos, M. E. G. Valerio, and R. A. Jackson, Appl. Phys. B: Lasers Opt. **81**, 841 (2005).
[29] A. A. Kaminskii, A. V. Butashin, J. Hulliger, P. Egger, S. N. Bagayev, H. J. Eichler, J. Findeisen, B. Liu, U. Täuber, P. Peuser, and S. N. Sulyanov, J. Alloys Compd. **275-277**, 442 (1998).
[30] N. Magnani, G. Amoretti, A. Baraldi, and R. Capelletti, Eur. Phys. J. B **29**, 79 (2002).
[31] A. Toncelli, M. Tonelli, A. Cassanho, and H. P. Jenssen, J. Lumin. **82**, 291 (1999).
[32] The lines (and transitions) are labeled by *Xn*, where $n=1,2,3,\ldots$ indicates the ground manifold sublevel (initial state of the absorption transition) and $X=\mathrm{A},\mathrm{B},\mathrm{C},\ldots$ indicates the sublevel within a given excited manifold (final state) (Ref. 21).
[33] G. Turrell, *Infrared and Raman Spectra of Crystals* (Academic, London, 1972), pp. 153–158.
[34] R. M. Macfarlane, A. Cassanho, and R. S. Meltzer, Phys. Rev. Lett. **69**, 542 (1992).
[35] N. I. Agladze and M. N. Popova, Solid State Commun. **55**, 1097 (1985).
[36] A. Baraldi, R. Capelletti, M. Mazzera, N. Magnani, I. Földvári, and E. Beregi, Phys. Rev. B **76**, 165130 (2007).
[37] G. Blasse, Int. Rev. Phys. Chem. **11**, 71 (1992).
[38] A. Baraldi, R. Capelletti, M. Mazzera, A. Ponzoni, E. Sani, and M. Tonelli, Radiat. Eff. Defects Solids **158**, 241 (2003).
[39] M. J. Weber, *Handbook of Optical Materials* (CRC, Boca Raton, 2003), p. 123.
[40] L. Pauling, Phys. Rev. **36**, 430 (1930).
[41] R. P. H. Gasser and W. G. Richards, *An Introduction to Statistical Thermodynamics* (World Scientific, Singapore, 1995), pp. 80–81.
[42] R. W. Dreyfus, Phys. Rev. **188**, 1340 (1969).